SAND2015-11103J

Synthesis and characterization of a series of Group 4 phenoxy-thiol derivatives.

Timothy J. Boyle,[*] Michael L. Neville,[a] and Marie V. Parkes[b]

Sandia National Laboratories, Advanced Materials Laboratory, 1001 University Boulevard, SE, Albuquerque, NM 87106

[a] *Present address:* Department of Chemistry, University of California, San Diego, 9500 Gilman Dr., La Jolla, CA

[b] *Geochemistry Department, Sandia National Laboratories, PO Box 5800, Albuquerque, NM 87185-0754*

*Author to whom correspondences should be sent at: ph (505)272-7625; fx (505)272-7336; e-mail tjboyle@Sandia.gov

Abstract. A series of Group 4 phenoxy-thiols were developed from the reaction products of a series of metal *tert*-butoxides ([M(OBu^t)$_4$]) with four equivalents of 4-mercaptophenol (H-4MP). The products were found by single crystal X-ray diffraction to adopt the general structure [(HOBu^t)(4MP)$_3$M(μ-4MP)]$_2$ [where M = Ti (**1**), Zr (**2**), Hf (**3**)] from toluene and [(py)$_2$M(4MP)] where M = Ti (**4**), Zr (**5**) and [(py)(4MP)$_3$Hf(μ-4MP)]$_2$ (**6**) from pyridine (py). Varying the [Ti(OR)$_4$] precursors (OR = *iso*-propoxide (OPr^i) or *neo*-pentoxide (ONep)) in toluene led to [(HOR)(4MP)$_3$Ti(μ-4MP)]$_2$ (OR = OPr^i (**7**), ONep (**8**)), which were structurally similar to **1**. Lower stoichiometric reactions in toluene led to partial substitution by the 4MP ligands yielding [H][Ti(μ-4MP)(4MP)(ONep)$_3$]$_2$ (**9**). Independent of the stoichiometry, all of the Ti derivatives were found to be red in color, whereas the heavier congeners were colorless. Attempts to understand this phenomenon led to investigation with a series of varied –SH substituted phenols. From the reaction of H-2MP and H-3MP (2-mercaptophenol and 3-mercaptophenol, respectively), the isolated products had identical arrangements: [(ONep)$_2$(2MP)Ti(μ,η^2-2MP)]$_2$ (**10**) and [(HOR)(3MP)M(μ-3MP)]$_2$ (M/OR = Ti/ONep (**11**); Zr/OBu^t (**12**)) with a similar red color. Based on the simulated and observed UV-vis spectra, it was reasoned that the color was generated due to a ligand-to-metal charge transfer for Ti that was not available for the larger congeners.

Keywords: alkoxides, thiols, titanium, zirconium, hafnium

1. Introduction

Thiol bearing metal precursors have found widespread use in the production of sulfur-based materials for such varied applications as power sources, [1, 2] metal-insulator-metal tunnel junctions,[3] optical,[1, 4] [5] advanced supports, [1, 2] catalytic, [1, 2] medical diagnosis/treatment,[6, 7] and even simple single-source precursors to metal-sulfide ceramics[1]. Of particular interest to our efforts is the development of highly soluble thiol-bearing precursors that will allow for the tuning of the index of refraction for plastic lenses[1, 4] [5] and for use as a protecting polymeric ceramic shell for nanomaterials[1, 2]. One approach that addressed both materials issues was to develop a family of metal alkoxide-thiol ($M(OR\text{-}SH)_x$) derivatives. For the Group 4 metals of interest,[3] a search of the literature[8] indicates there are very few crystallographically characterized $[M(OR\text{-}SH)_4]_n$ derivatives available that could be applied to these problems. Therefore, we undertook the synthesis and characterization of a set of $[M(OR)_{4-x}(O\text{-}R\text{-}SH)_x]_n$ precursors, focusing on 4-mercaptophenol (H-4MP) derivatives. The reaction was found to proceed as shown in Eq 1 with a variety of $[M(OR)_4]$ (where OR = OPr^i ($OCH(CH_3)_2$), OBu^t ($OC(CH_3)_3$), and ONep ($OCH_2C(CH_3)_3$)).

$$\mathbf{[M(OR)_4] + \mathit{x}\,H\text{-}4MP \xrightarrow{solv} [M(OR)_{4-x}(4MP)_x(solv)_y] + \mathit{x}\,H\text{-}OR} \qquad \mathbf{(1)}$$

M = Ti, Zr, Hf; OR = OBu^t, ONep; x = 2 or 4; solv = tol, py

The products were identified as $[(HOBu^t)(4MP)_3M(\mu\text{-}4MP)]_2$ where M = Ti (**1**), Zr (**2**), Hf (**3**), from toluene and $[(py)_2M(4MP)]$ where M = Ti (**4**), Zr (**5**) and

$[(py)(4MP)_3Hf(\mu\text{-}4MP)]_2$ (**6**) from pyridine (py). Using different $[Ti(OR)_4]$ precursors led to the isolation of $[(HOR)(4MP)_3Ti(\mu\text{-}4MP)]_2$ (OR = OPr^i (**7**), ONep (**8**) and different stoichiometries yielded $[H][Ti(\mu\text{-}4MP)(4MP)(ONep)_3]_2$ (**9**). Since the 4MP-modified $[Ti(OR)_4]$ derivatives were found to be red in color and the heavier congeners were colorless, a series of varied –SH substituted phenols (H-2MP and H-3MP) were also investigated as modifiers to explore the origins of this phenomenon. From the reaction of H-2MP and H-3MP (2-mercaptophenol and 3-mercaptophenol, respectively), the isolated products had identical arrangements, which were identified as $[(ONep)_2(2MP)Ti(\mu,\eta^2\text{-}2MP)]_2$ (**10**) and $[(HOR)(3MP)M(\mu\text{-}3MP)]_2$ (M = Ti, OR = ONep (**11**); Zr, OBu^t (**12**)).

2. Material and Methods

All compounds described below were handled with rigorous exclusion of air and water using standard Schlenk line and glove box techniques unless otherwise discussed. All solvents (anhydrous Sure/Seal™) and chemicals were used as received (Aldrich) without further purification, including: toluene (tol), pyridine (py), H-4MP, $[Ti(OPr^i)_4]$, $[M(OBu^t)_4]$ M = Ti, Zr, Hf. $[Ti(\mu\text{-}ONep)(ONep)_3]_2$ [9] and $[M_2(ONep)_8(HOBu^t)]$ (M = Zr, Hf referred to as $[Zr(ONep)_4]$ and $[Hf(ONep)_4]$, respectively)[10] were synthesized according to literature procedures.

Analytical data was collected on dried crystalline samples. FTIR data were collected on a Nicolet 6700 FTIR spectrometer using a KBr pellet press under a flowing atmosphere of nitrogen. Elemental analyses were collected on a Perkin Elmer 2400 Series II CHNS/O Analyzer with samples prepared in an argon-filled

glovebox. Thermal gravimetric analysis (TGA) data were collected on a Mettler Toledo TGA/DSC 1 STAR^e System instrument at 5 ^{o}C/min ramp rate under a flowing argon atmosphere to 650 ^{o}C. NMR samples were dried, dissolved in the appropriate deuterated solvent, and flame sealed in an NMR tube under vacuum. UV-visible (UV-vis) spectra were collected on a Cary 400 Scan UV-Visible Spectrophotometer. NMR spectra were collected on a Bruker Avance-III 500 NMR spectrometer under standard experimental conditions. ^{1}H NMR analyses were performed with a 4-second recycle delay at 16 scans; spectra were referenced to the residual proton in toluene-d_8 (tol-d_8) or pyridine-d_5 (py-d_5).

2.1. General reaction.

To a stirring solution of the appropriate [M(OR)$_4$] in the desired solvent (tol or py), four equivalents of H-4MP ligand were added. The mixture was stirred for a minimum of 12 h and then set aside with the cap loose to allow the volatile component to evaporate, until crystals formed. If a precipitate formed during the initial mixing, the sample was heated until the solution went clear and then the reaction mixture was set-aside until crystals formed (on the order of hours). Yields reported are from the first batch of crystals isolated and were not optimized.

2.1.1 [(HOBu^t)(4MP)$_3$Ti(μ-4MP)]$_2$ (1). [Ti(OBu^t)$_4$] (0.500 g, 1.47 mmol), H-4MP (0.741 g, 5.88 mmol) in tol (~5 mL). Reaction turns dark red upon mixing. Yield 85.5% (0.840 g). FTIR (KBr, cm^{-1}) 3025(w), 2978(w), 2561(w), 2388(w), 2152(w), 1880(w), 1584(m), 1483(s), 1449(m), 1389(m), 1367(m), 1278(s), 1257(s),

1246(s), 1222(s), 1164(m), 1097(m), 1009(w), 899(s), 860(m), 825(s), 734(w), 718(m), 711(m,sh), 688(m), 667(m), 636(w), 558(m), 478(m), 456(m). ^{1}H NMR was not obtained (*vide infra*). Elemental Analysis calc'd for $C_{28}H_{30}O_5S_4Ti$ (MW = 622.65): C%, 54.01; H%, 4.86. $C_{63}H_{68}O_{10}S_8Ti_2$ (MW = 1337.44; **1** + tol): C%, 56.58; H%, 5.12. Found: C%, 56.77; H%, 5.09.

[(HOBu^t)(4MP)$_3$Zr(μ-4MP)]$_2$ (**2**). [Zr(OBu^t)$_4$] (0.500 g, 1.30 mmol), H-4MP (0.658 g, 5.21 mmol) in tol (~5 mL). Yield 88.6% (0.769 g). FTIR (KBr, cm^{-1}) 3340(w, br), 3054(w), 2921(w), 2850(w), 2347(w), 2171(w,br), 1605(m), 1503(s), 1443(m), 1285(s), 1252(s), 1164(w), 1092(w), 1041(w), 876(m), 831(m), 787(m), 702(w), 607(w), 550(m), 521(m), 461(w). ^{1}H NMR (500.18 MHz, tol-d_8) δ 7.31 (1H, d, $J_{H\text{-}H}$ = 4.0 Hz. OC$_6$*H*$_4$SH), 7.00 (2H, d, $J_{H\text{-}H}$ = 4.0 Hz. OC$_6$*H*$_4$SH), 6.20 (1H, s, OC$_6$*H*$_4$SH), 6.01 (2H, d, $J_{H\text{-}H}$ = 4.0 Hz. OC$_6$*H*$_4$SH), 3.12 (1H, s, OC$_6$H$_4$S*H*), 3.01(1H, s, OC$_6$H$_4$S*H*), 2.92(2H, s, OC$_6$H$_4$S*H*), 1.15 (9H, s, HOC(C*H*$_3$)$_3$, 1.03 (5H, s, HOC(C*H*$_3$)$_3$). Elemental Analysis calc'd for $C_{56}H_{60}O_{10}S_8Zr_2$ (MW = 1332.01): C%, 50.50; H%, 4.54. Found: C%, 51.14; H%, 4.63.

[(HOBu^t)(4MP)$_3$Hf(μ-4MP)]$_2$ (**3**). [Hf(OBu^t)$_4$] (0.500 g, 1.06 mmol), H-4MP (0.535 g, 4.24 mmol) in tol (~5 mL). Yield 69.7% (0.592 g). FTIR (KBr, cm^{-1}) 3025(w), 2979(w), 2388(m), 2348(w), 2175(w), 1879(w), 1590(s), 1572(w,sh), 1370(w), 1299(s), 1274(s), 1250(s), 1213(s), 1166(m), 1096(w), 1028(w), 1012(w), 890(m), 858(m), 827(s), 734(w), 705(m), 685(w), 665(m), 637(w), 546(w), 480(m), 464(m), 423(w), 413(w). ^{1}H NMR (500.18 MHz, tol-d_8) δ 7.32 (1H, d, $J_{H\text{-}H}$ = 4.0 Hz, OC$_6$*H*$_4$SH), 7.09(2H, d, $J_{H\text{-}H}$ = 4.0 Hz, OC$_6$*H*$_4$SH), 6.88 (1H, d, $J_{H\text{-}H}$ = 4.0 Hz, OC$_6$*H*$_4$SH), 6.84 (1H, d, $J_{H\text{-}H}$ = 4.0 Hz , OC$_6$*H*$_4$SH), 6.20 (1H, s, OC$_6$*H*$_4$SH), 6.03(1H, d, $J_{H\text{-}H}$ = 4.0 Hz, OC$_6$*H*$_4$SH),

3.12 (1H, s, OC_6H_4SH), 3.00(1H, s, OC_6H_4SH), 2.93(1H, s, OC_6H_4SH), 2.91 (1H, s, OC_6H_4SH), 1.09 (4H, s, $HOC(CH_3)_3$, 1.03 (3H, s, $HOC(CH_3)_3$). Elemental Analysis calc'd for $C_{63}H_{68}Hf_2O_{10}S_8$ (MW = 1598.69; **3** + tol): C%, 47.33; H%, 4.29. Found: C%, 47.04; H%, 4.27.

[(py)$_2$Ti(4MP)$_4$] (**4**). [$Ti(OBu^t)_4$] (0.500 g, 1.47 mmol), H-4MP (0.741 g, 5.88 mmol) in py (~3 mL). Reaction turns dark red upon mixing. Yield 61.2% (0.716 g). FTIR (KBr, cm^{-1}) 3020(w), 2386(w), 2346(w), 2141(w,br), 1602(m), 1582(m), 1481(s), 1443(m), 1287(s,sh), 1254(s), 1216(s), 1166(m), 1096(m), 1068(w), 1041(w), 1010(w), 890(m), 870(m), 822(s), 757(w), 698(s), 675(w), 632(w), 562(w), 495(s). ^{1}H NMR (500.18 MHz, py-d_5) δ 8.71 (py), 7.78 (py), 7.34 (py), 7.05 (2H, s, OC_6H_4SH), 6.41 (2H, s, OC_6H_4SH), 3.40 (1H, s, OC_6H_4SH). Elemental Analysis calc'd for $C_{34}H_{30}N_2O_4S_4Ti$ (MW = 706.73): C%, 57.78; H%, 4.28; N%, 3.96. Found: C%, 57.49; H%, 4.31; N%, 3.98.

[(py)$_2$Zr(4MP)$_4$] (**5**). [$Zr(OBu^t)_4$] (0.500 g, 1.30 mmol), H-4MP (0.658 g, 5.21 mmol) in py (~3 mL). Yield 66.4% (0.662 g). FTIR (KBr, cm^{-1}) 3066(w), 3021(w), 2559(w), 2152(w), 1872(w), 1736(w), 1647(w), 1604(w), 1586(s), 1561(w,sh) 1484(s), 1444(s), 1403(w), 1272(s), 1210(m), 1165(m), 1094(m), 1069(m), 1042(m), 1011(m), 872(s), 825(s), 758(m), 694(s), 664(m), 634(m), 544(w), 511(m), 486(m), 458(m). ^{1}H NMR (500.18 MHz, $CDCl_3$) δ 8.65 (py), 7.88 (py), 7.51 (py), 7.24 (2H, d, J_{H-H} = 3.5 Hz, OC_6H_4SH), 6.87 (2H, d, J_{H-H} = 3.5 Hz, OC_6H_4SH), 3.47 (1H, s, OC_6H_4SH). Elemental Analysis calc'd for $C_{34}H_{30}N_2O_4S_4Zr$ (MW = 750.09): C%, 54.44; H%, 4.03; %N, 3.73. Found: C%, 54.34; H%, 4.04; N%, 3.75

[(py)(4MP)$_3$Hf(μ-4MP)]$_2$ (**6**). [Hf(OBu^t)$_4$] (0.500 g, 1.06 mmol), H-4MP (0.535 g, 4.24 mmol) in py (~5 mL). Crystals were isolated from a concentrated py solution with a toluene layered on top. Yield 66.0% (0.531 g). FTIR (KBr, cm^{-1}) 3022(w), 2550(w), 1606(w), 1586(m), 1561(w), 1485(s), 1443(m), 1308(m), 1270(s), 1209(m), 1166(m), 1095(m), 1068(m), 1043(m), 1011(w), 877(m), 824(s), 756(w), 659(s), 662(m), 634(m), 550(w), 467(m), 455(m). ^{1}H NMR (500.18 MHz, $CDCl_3$) δ 8.54 (py), 7.86 (py), 7.31 (py), 7.24 (2H, d, $J_{H\text{-}H}$ = 3.5 Hz, $OC_6\mathit{H}_4SH$), 6.75 (2H, d, $J_{H\text{-}H}$ = 3.5 Hz, $OC_6\mathit{H}_4SH$), 3.51 (1H, s, $OC_6H_4S\mathit{H}$). Elemental Analysis calc'd for $C_{29}H_{25}HfNO_4S_4$ (MW = 758.25); C%, 45.94; H%, 3.32; N%, 1.85. $C_{63}H_{55}Hf_2N_3O_8S_8$ (**6**+1 py; MW = 1595.63): C%, 47.42; H%, 3.47; N%, 2.63. Found: C%, 47.72; H%, 3.51; N%, 2.35

[(HOPr^i)(4MP)$_3$Ti(μ-4MP)]$_2$ (**7**). [Ti(OPr^i)$_4$] (0.500 g, 1.76 mmol), H-4MP (0.887 g, 7.04 mmol) in tol (~5 mL). Reaction turns dark red upon mixing. Yield 59.7% (0.639 g). FTIR (KBr, cm^{-1}) 3020(w), 2969(w), 2569(w), 1879(w), 1585(m), 1482(s), 1401(w), 1277(s), 1252(s), 1219(s), 1165(m), 1010(w), 899(s), 857(m), 822(s), 711(s), 689(m), 669(m), 636(w), 562(m), 494(m), 416(m). ^{1}H NMR (500.18 MHz, $CDCl_3$) δ 7.57 (2H, mult., $OC_6\mathit{H}_4SH$), 7.09, 6.98, 6.82 (5H, mult., $OC_6\mathit{H}_4SH$ and toluene), 6.63(2H, mult. $OC_6\mathit{H}_4SH$), 4.26 (4H, sept, $J_{H\text{-}H}$ = 5.0 Hz, $OC\mathit{H}(CH_3)_2$), 2.95 (2H, s, $OC_6H_4S\mathit{H}$) 0.95 (14H, d, $J_{H\text{-}H}$ = 5.0 Hz, $OCH(C\mathit{H}_3)_2$). Elemental Analysis calc'd for $C_{27}H_{28}O_5S_4Ti$ (MW = 608.62): C%, 53.28; H%, 4.64. Found: C%, 53.05; H%, 4.77.

[(HONep)(4MP)$_3$Ti(μ-4MP)]$_2$ (**8**). [Ti(ONep)$_4$]$_2$ (0.500 g, 0.631 mmol), H-4MP (0.637 g, 5.05 mmol) in tol (~5 mL). Reaction turns dark red upon mixing. Yield 85.9% (0.690 g). FTIR (KBr, cm^{-1}) 3383(s), 3075(m), 2962(s), 2924(s), 2857(s),

2559(m), 1582(m), 1483(s), 1402(w), 1384(w), 1259(s), 1164(m), 1095(m), 1012(m), 903(m), 826(s), 787(m), 615(w), 572(w), 490(m), 137(w). ^{1}H NMR(500.18 MHz, tol-d_8) δ 6.88 (8H, d, J_{H-H} = 5.0 Hz, OC_6H_4SH), 6.29 (8H, s(br), OC_6H_4SH), 3.17 (3H, s, OC_6H_4SH), 2.94 (4H, s, $HOCH_2C(CH_3)_3$), 0.74 (14H, s, $HOCH_2C(CH_3)_3$). Elemental Analysis calc'd for $C_{29}H_{32}O_5S_4Ti$ (MW = 636.68): C%, 54.71; H%, 5.07. Found: C%, 55.26; H%, 5.11.

[H][Ti(μ-4MP)(4MP)(ONep)$_3$]$_2$ (**9**). $[Ti(ONep)_4]_2$ (0.500 g, 0.631 mmol), H-4MP (0.319 g, 2.52 mmol) in tol (~5 mL). Yield 82.3% (0.490 g). FTIR (KBr, cm^{-1}) 3201(w), 2953(m), 2902(w), 2866(m), 2559(w), 1586(m), 1485(s), 1393(w), 1363(m), 1254(s), 1234(s), 1163(m), 1097(s), 1024(m), 1011(m), 935(w), 899(w), 856(m), 835(m), 750(w), 691(s), 566(w), 485(m). ^{1}H NMR was not obtained (vide infra). Elemental Analysis calc'd for $C_{27}H_{44}O_5S_2Ti$ (MW = 560.23): C%57.84; H%, 7.91; $C_{22}H_{32}O_4S_2Ti$ (MW = 472.48): (**9** - HONep): C%, 55.93; H%, 6.83. Found: C%, 55.38; H%, 7.37.

[(ONep)$_2$(2MP)Ti(μ,η^2-2MP)]$_2$ (10). $[Ti(ONep)_4]_2$ (0.500 g, 0.631 mmol), H-2MP (0.319 g, 2.53 mmol) in tol (~5 mL). Reaction turns dark red upon mixing. Yield 17.11% (0.102 g). FTIR (KBr, cm^{-1}) 3021(w), 2952(m), 2901(w), 2865(w), 2563(w), 2509(w), 1568(m), 1466(s), 1438(s), 1396(m), 1364(m), 1285(m), 1264(s), 1243(s), 1223(s), 1128(w), 1080(s), 1032(m), 1001(m), 935(w), 902(w), 870(m), 848(m), 754(m), 743(s), 704(m), 690(m), 624(m), 608(m), 555(w), 514(w), 474(w), 408(m). ^{1}H NMR was not obtained (vide infra). Elemental Analysis calc'd for $C_{22}H_{32}O_4S_2Ti$ (MW = 472.48): C%, 55.93; H%, 6.83. Found: C%, 56.19; H%, 6.89.

[(HONep)(3MP)$_3$Ti(μ-3MP)]$_2$ (11). [Ti(ONep)$_4$]$_2$ (0.500 g, 0.631 mmol), H-3MP (0.638 g, 5.05 mmol) in tol (~5 mL). Reaction turns dark red upon mixing. Yield 51.2% (0.411 g). FTIR (KBr, cm^{-1}) 3029(w), 2955(w), 2865(w), 2558(w), 2364(w), 2344(w), 1578(s), 1468(s), 1419(s), 1365(w), 1297(s), 1240(s), 1158(m), 1095(s), 1070(m), 1038(w), 997(m), 945(s), 889(m), 859(w), 773(m), 729(w), 681(m), 651(w), 604(w), 584(w), 507(w), 473(w), 446(m). ^{1}H NMR was not obtained (vide infra). Elemental Analysis calc'd for $C_{29}H_{32}O_5S_4Ti$ (MW = 636.68): C%, 54.71; H%, 5.07. $C_{24}H_{20}O_4S_4Ti$ (MW = 548.53, **11** - HONep): C%, 52.55; H%, 3.68. Found: C%, 51.96; H%, 4.06.

[(HOBu^t)(3MP)$_3$Zr(μ-3MP)]$_2$ (12). [Zr(OBu^t)$_4$] (0.500 g, 1.30 mmol), H-3MP (0.658 g, 5.21 mmol) in tol (~5 mL). Yield 60.6% (0.526 g). FTIR (KBr, cm^{-1}) 3310(s), 3058(s), 2971(s), 2560(s), 1918(m), 1731(m), 1580(s), 1473(s), 1520(s), 1370(m), 1272(s), 1245(s), 1215(m), 1157(m), 1095(m), 1014(w), 996(w), 942(s), 888(m), 856(w), 776(m), 747(w), 715(w), 638(m), 613(w), 600(w), 536(w), 482(m), 445(w), 410(m). ^{1}H NMR was not obtained (vide infra). Elemental Analysis calc'd for $C_{28}H_{30}O_5S_4Zr$ (MW = 666.01): C%, 50.50; H%, 4.54. Found: C%, 50.03; H%, 4.61.

2.2. General X-ray Crystal Structure Information.

Single crystals were mounted onto a loop from a pool of Fluorolube™ and immediately placed in a cold N_2 vapor stream, on a Bruker AXS diffractometer employing an incident-beam graphite monochromator, MoKa radiation (λ = 0.71070 Å) and a SMART APEX CCD detector. Lattice determination and data collection were carried out using SMART Version 5.054 software. Data reduction was performed

using SAINTPLUS Version 6.01 software and corrected for absorption using the SADABS program within the SAINT software package. Structures were solved by direct methods or by using the intrinsic (SHELXT) method that yielded the heavy atoms, along with a number of the lighter atoms. Subsequent Fourier syntheses yielded the remaining light-atom positions. The hydrogen atoms were fixed in positions of ideal geometry and refined using SHELXL within the OLEX2 program.[11] The final refinement of each compound included anisotropic thermal parameters for all non-hydrogen atoms. All final CIF files were checked using the CheckCIF program (http://www.iucr.org/). Additional information concerning the data collection and final structural solutions can be found in the supplemental information or by accessing CIF files through the Cambridge Crystallographic Data Base. Table 1 lists the data collection parameters for the structurally characterized compounds **1** – **12**. Table 2 tabulates the metrical data isolated in this work. Specific issues that arose with the various crystal structure solutions are discussed below.

Disordered lattice solvent molecules that could not be modeled were 'squeezed'[12] for compounds **1** (490.0 $Å^3$, 1 toluene), **3** (662.1 $Å^3$, 1 toluene), and **8** (508.5 $Å^3$, 1 toluene). EADP was used for **9**, C(3) to C(8); for **10**, C(1) to C(1a) and C(3) to C(5a). In addition, for the final structure of **10**, positional disorder in the 2MP ligand was successfully modeled by PART instructions and AFIX 66 was used on C(1)-C(6) and C(1a)-C(6a) (hexagon construction). For compound **11**, the disorder noted for the 3MP rings leads to a high final R-value and unreliable metrical data; however, connectivity is unequivocally established. For compound

12, the crystal structure isolated had substitutional disorder. The symmetry and orientation of the pendant ligands are arranged such that one of the positions is split between a OBu^t and a 3MP group at a 60:40% ratio. For the disorder noted above, a specific conformation is shown in the various figures.

2.3. Molecular Modeling.

Time-dependent density functional theory (TD-DFT) calculations, as implemented in the Gaussian program,[13] were used to predict UV-vis spectra of four model complexes: (a) **1**, (b) **4**, and two analogs of the py-coordinated Ti complexes, with either (c) electron-withdrawing (**EW**) or (d) electron donating (**ED**) groups on the aromatic rings. For **1** and **4**, initial atomic coordinates were taken from the solved crystal structures, then optimized using the PBE0[14-16] functional (the 1996 functional of Perdew, Burke, and Ernzerhof, as hybridized by Adamo). The LANL2DZ effective core potential basis set[17-19] was used on Ti; all other atoms were described using the 6-31G* basis set.[20-22] For **EW** and **ED**, the initial geometries were built by replacing hydrogen atoms in the 3- and 5-positions on the mercaptophenol rings with either cyano groups or methoxy groups, respectively, then optimizing the geometries as described for **1** and **4**. After the geometries had been optimized, time-dependent density functional theory calculations[23-25] were undertaken to determine the energies and intensities of the 50 lowest-energy electronic transitions for each complex. Care was taken to ensure that all of the excited states that would be expected to cause absorption in the visible part of the spectrum were examined. The UV-vis spectra were calculated using the SWizard

program, revision 5.0,[26-28] using the Gaussian model with half-widths of 3000 cm^{-1}.

3. Results and Discussion

A search of the crystallographically characterized compounds[8] that possess a MO_4 unit (M = Ti, Zr, Hf) as well as four S-H groups, yields only 3 compounds: $[Zr(4MP)_6]^{2-}[HN(CH_2CH_3)_3]^{2+}\bullet C_6D_6$,[29] $[M_{12}(\mu_3\text{-}O)_8(\mu_3\text{-}OH)_8(MPA)_{24}\bullet n(H\text{-}MPA)]$ where M = Zr (n = 4), Hf (n = 5) and MPA = $O_2C(CH_2)_2SH$ [4]. Due to the limited number of precursors available, the synthesis and characterization of a series of $[M(OR\text{---}SH)_4]$ was initiated. A survey of H-OR---SH ligands coupled with our previous experience with the H-4MP ligand and the high solubility of these derivatives,[30] led us to focus on generating the homoleptic $[M(4MP)_4]$ precursors as shown in Eq 1. The following details the characterization of these compounds, followed by the impact that they had on the final polymeric species generated therefrom.

3.1 Synthesis.

The initial reactions attempted focused on modifying the OBu^t derivatives, since each of the Group 4 $[M(OBu^t)_4]$ precursors were highly soluble in organic solvents and were commercially available. Additional efforts focused on the impact of the: 4MP ligand (sub-section 3.1.1), solvent (3.1.2), alkoxide chain (3.1.3), stoichiometry (3.1.4), and alternative SH-aryl substitutions (3.1.5; i.e., H-2MP, H-3MP) on the final structures obtained.

3.1.1. 4MP ligand.

The first reactions were undertaken as written in Eq 1 with x = 4 using toluene as the solvent. Upon introduction of the H-4MP to [M(OBu^t)$_4$], the mixture turned dark red when M = Ti, while the Zr and Hf analogs remained colorless. After stirring for 12 h, the reactions were set aside and the volatile component was allowed to slowly evaporate. X-ray quality red (Ti) and colorless (Zr, Hf) crystals were isolated. Table 1 lists the data collection parameters for these structures. FTIR spectra on the dried crystalline material clearly showed the loss of OBu^t ligands and the incorporation of the 4MP ligand. In each spectrum, a small OH stretch around 3200 cm^{-1}, aromatic stretches for the C-H bonds around 3025 cm^{-1}, and in-ring C-C stretches between 1615 and 1400 cm^{-1} were observed. In addition, the appropriate OBu^t bends and stretches were present. Small S-H stretches of the 4MP-modified compounds ranged from 2550 to 2059 cm^{-1}; this represents a shift from literature reports of S-H stretch range (2600-2400 cm^{-1});[7] however, the SH peak for the H-4MP ligand was not readily evident in the experimental or literature[31] FTIR spectral data.

In addition, UV-vis spectra were collected for the various 4MP-modified complexes. As mentioned, upon complexation of the 4MP ligand to the metals, a deep red color was noted for **1**, with a maximum absorption observed 252 and 345 nm for **1**; in contrast, a pale yellow color was observed for **2** and **3** with a small absorbance maximum at ~285 nm. Quantum calculations were undertaken to further investigate the different colors noted (*vide infra*).

To assist in elucidating the reaction product, single crystal X-ray diffraction studies were undertaken for the isolated crystalline products. Independent of the metal employed, each sample was found to adopt the dinuclear $[(HOBu^t)(4MP)_3M(\mu\text{-}4MP)]_2$ complex. Figures 1 -3 show the structures of **1** - **3**, respectively. Each metal center was solved in a pseudo-octahedral (*OC*-6) geometry using two μ-4MP and three terminal 4MP ligands. The final coordination site was filled by a OBu^t moiety. A search of the literature[32] indicates that the M-OBu^t bond lengths (M = Ti 1.8, Zr or Hf = 1.9 Å) reported in the literature [33] are shorter than the M-OBu^t distances noted for **1** - **3** (see Table 2). The structure literature only reports one Group 4 metal-$HOBu^t$ (Hf-$HOBu^t$ = 2.275 Å),[34] which is in agreement with the distances noted for **3**. This suggests the OBu^t in **1** - **3** are protonated, even though the quality of the structure does not show the presence of the H atom. Furthermore, this solvation is consistent with the –OH stretch in the FTIR spectrum.

3.1.2. solvent.

To further verify whether a H-OBu^t moiety was solvating the metals, the reaction (Eq 1) was repeated using the same $[M(OBu^t)_4]$ precursors in pyridine solution rather than toluene. It was expected that the $HOBu^t$ would be replaced by the pyridine. Again, the Ti system yielded red solutions and crystals; whereas, the larger congeners were pale yellow. It is of note that crystals took a substantially longer time to grow, presumably due to the higher solubility in the py compared to the tol solvent system. FTIR data concerning the dried crystalline material clearly

showed exchange of the OBu^t for the 4MP ligand as well as incorporation of py solvent molecules. UV-vis spectra for these products were consistent with those recorded in toluene.

Again, isolation of the crystals allowed for exploration of structural properties using single crystal X-ray studies. For the lighter congeners (**4** and **5** shown in Figures 4 and 5, respectively), the compounds were monomeric using four 4MP ligands and two additional py solvent molecules to generate the pseudo *OC*-6 geometry. In contrast, the Hf derivative **6** (Figure 6) was the py solvated dinuclear species originally anticipated. These crystal structures, especially **6**, support the H-OBu^t assignment in **1** - **3**, as the alcohol is not present in any of these structures, whereas any alkoxide should have been maintained upon dissolution in pyridine. The metrical data for the M-4MP-py derivaitves are similar to those noted for **1** – **3**. The M-py bonds are as expected longer than those noted for the M-(HOBu^t) but in-line with reported literature M-py (M = Ti, Zr, Hf) distances. [3, 32]

3.1.3. alkoxide chain.

A further study using different OR groups focused on the smaller OPr^i and the larger ONep derivatives. Mixing of the [Ti(OR)$_4$] with four equivalents of H-4MP ligand (Eq 1) led to a red solution and red crystals for both R= OPr^i and R=ONep. The FTIR spectra again showed an exchange had occurred with the presence of a small OH stretch. Single crystal structural solutions revealed the dinuclear, fully exchanged complex with each pseudo-*OC*-6 coordination of the Ti metal centers completed through the binding of an HOR (HOR = HOPr^i (**7**, Figure 7) and HONep (**8**,

Figure 8). The metrical data of **7** – **8** were consistent with each other, compounds **1** – **3**, and literature values.[32]

3.1.4. stoichiometry.

Reducing the stoichiometry of H-4MP in Eq 1 from 4 equivalents to 2 equivalents per metal center using $[Ti(ONep)_4]_2$, led to the isolation of the red colored **9**, which by FTIR possessed HO-. Single crystal structure solutions (see Figure 9) indicated that the dinuclear structure was formed with a pseudo-*OC*-6 metal center. This is generated by two μ-4MP, one terminal 4MP, and three terminal ONep ligands per metal. Based on the previous HOR solvates, one of the ligands is considered H-ONep; however, location of the proton could not be made and is considered disordered over the entire molecule. This is represented by the '[H]' in front of the formula. The metrical data is consistent with the other Ti-4MP structures (*vide infra*) and the Ti-ONep distances are in agreement with the parent $[Ti(\mu\text{-}ONep)(ONep)_3]_2$ distances and angles.[9] This demonstrates that the degree of substitution by the 4MP ligand can be managed by the stoichiometry used in the initial reaction.

3.1.5. alternative SH-aryl substitution.

Further investigations using other substituted thiol phenols were undertaken to determine their structural impact and color variations. The commercially available H-2MP and H-3MP ligands were used in similar reactions as noted for Eq 1. Again, for the Ti systems, the solution and resulting crystals were

red, while the Zr and Hf derivatives were colorless. This indicates that the location of the –SH group on the ring, had little impact on the overall color of the resulting complex. An analysis of the crystalline material revealed some interesting results for the 2MP derivative. As shown in Figure 10, a dinuclear species was isolated for **10**, with one of the 2MP acting as a bridging chelating ligand filling the open CN-6 site. Another μ_c-2MP, two ONep and one 2MP ligand fill the remaining coordination sites. The terminal Ti-ONep distances range from 1.75 to 2.17 Å which exceeds the limits of the reported 'Ti(ONep)$_4$' distances reported (1.74 to 1.84 Å).[9, 34] The longer distanced Ti-O bond is *trans* to the aryloxide 3MP ligand but substantially shorter distances were reported for *trans* ONep/OAr structures.[35-37] The terminal (1.89 Å) and bridging (2.06 Å) Ti-O of the 3MP ligands are consistent with literature reported diphenoxide species; Ti-S distance (2.369 Å) of **10** is much longer than any other 'S-TiO$_3$' moieties reported in the literature (1.76 to 2.18 Å).[3]

As the thiol ligand was moved further away from the metal center using the 3MP, the similarly arranged products **11** and **12** (Figures 11 and 12, respectively) were identified as parent, HOR, solvated dimers as observed for the 4MP derivatives. It is of note that the structure of **11** was solved with significant disorder in the 3MP ligands, which prevented the dissemination of reliable metrical data; however, the structure was unequivocally established and is presented here for completeness. The change of the thiol location did not alter the metrical data of the dimer as compared to its 4MP analog **2**.

3.2. Elemental Analysis.

Elemental analyses of **1** - **12** were undertaken to assist in determining the purity of the dried crystalline powders. Typically, $[M(OR)_4]$ do not yield acceptable elemental analyses by thermal processing due to the properties that make them of interest for materials production (i.e., high volatility, rapid hydrolysis and condensation, low decomposition temperatures, etc.). Further, when solvents are bound to the metal, their premature loss or inclusion of spurious solvent molecules can lead to complications in determining the elemental composition. Therefore, it was surprising that the analyses of the bulk powders for **1** - **12** were found to be acceptable. Acceptable analyses were obtained for **1** and **3**, by adding the 'squeezed' molecule of toluene; for **6**, the inclusion of a py molecule; for **9**, the loss of an H-ONep molecule. In general, the elemental analyses of the bulk powders were consistent with the single crystal structures. The stability of these compounds must be associated with the 4MP ligands.

3.3. Solution Behavior.

With established pure powders, solution state NMR (2.3.1) and UV-vis spectroscopy (2.3.2) were undertaken to further characterize compounds **1** – **12**.

3.3.1. solution state NMR spectroscopy.

The ^{1}H NMR spectra for **1** - **3** were collected in toluene-d_8. For **1**, no meaningful spectrum could be obtained due to the low solubility of the complex. Other solvents were attempted and did not increase the information obtained. For **2**, the number of aryl (4) and S-H (3) resonances observed indicates that the ligands

are effectively blocked from free rotation (i.e., locked out). The expected 8 methylene aromatic resonances for the locked out dimer overlap with each other and/or are obfuscated by the residual toluene resonances, which results in the presence of four doublets that account for 6 of the protons. Three thiol proton resonances were observed in a 1:1:2 ratio representing the bridging, axial, and two overlapping equatorial S-H resonances. The bound HOBu^t resonances approach a 2:1 ratio, which is consistent with inequivalent methyl resonances probably due to the restricted rotation. For **3** a similar spectrum was observed; however, 7 of the 8 phenoxide resonances can be clearly observed along with four distinct S-H resonances in a 1:1:1:1 ratio. The methyl resonances of the OBu^t are also present and appear to be in an approximate 1:1 ratio. In general, from these spectra it is apparent the dinuclear complex with restricted rotation of the methyl groups is retained in solution.

If a Lewis basic solvent is employed, a new complex is formed (i.e., **4** – **6** in pyridine). Thorough analysis of the solution behavior of **4** - **6** in the parent solvent py-d_8 was again problematic due to overlapped aromatic resonances. Proton NMR data are included for **4** in py-d_5 and **5** and **6** in $CDCl_3$. One S-H resonance was observed for each sample, which implies the monomeric species were maintained upon dissolution. For **7** and **8**, full interpretation is limited due to the overlap of the 4MP phenyl protons and the residual toluene. The broad resonances of the peaks indicate significant ligand exchange with equated phenoxy resonances and thiols. In addition, the resonances associated with the bound alcohols are present; however,

the amount of HOPr^i and HONep ligands is much larger than expected which may be due to preferential dissolution of the bound HONep over that of metal complex.

Based on the asymmetry and alkoxide ligands employed, NMR spectra for **9** – **12** were expected to be difficult to obtain and more complex than those noted for **1** – **8**. This proved to be true and little useful information concerning the solution behavior of these compounds could be discerned and thus was not included. In general, it appears that the unsolvated, dinuclear species observed in the solid state were retained in solution with locked out ligands. The pyridine adducts also maintain their monomeric nature but appear to be less restricted in their ligand arrangement.

3.3.2 UV-vis spectroscopy.

UV-vis spectra were collected for the various Ti based compounds, as the colorless Zr and Hf derivatives would not display a strong absorbance. A variety of solvents were investigated, including dimethyl formamide, pyridine, and toluene. Using toluene as the solvent was found to yield the most informative spectra. These are shown in Figure 13 for the dinuclear species **1** and monomeric complex **4** which were selected to represent the structure types available. As can be discerned, the absorbance spectra look similar with one sharp and one broad absorption around 252 and 345 nm, respectively, for **1** and 301 and 365 nm, respectively, for **4**. In order to further interpret these, additional information was obtained through computational calculations.

3.4. Computational Calculations.

Since limited information pertaining to the source of the color for the Ti species and lack of color for the Zr and Hf species could be derived from the structural properties or analytical data, computational calculations were undertaken. UV-vis spectra for the heavier congeners were not predicted due to limitations in the methods used for 2nd and 3rd row transition metals. For Ti-containing complexes, UV-Vis spectra were predicted using the time-dependent density functional theory for four model complexes (see Figures 14-i), including (a) **1** (dimer) and (b) **4** (monomer) along with theoretical compounds with either (c) electron-withdrawing (**EW**) or (d) electron-donating (**ED**) groups on the 4-MP rings. These compounds were included to determine if the differences in UV-vis spectra could be attributed to the electron donation of the thiophenol ring (ligand-to-metal charge transfer). Time-dependent density functional theory calculations[23-25] were undertaken on optimized structures to determine the energies and intensities of the 50 lowest-energy electronic transitions for each complex. The UV-vis spectra were calculated and all of the excited states that would be expected to cause absorption in the visible part of the spectrum were examined. The predicted spectra are shown in Figure 14-ii.

It was expected that any red-colored complex should have significant absorbance between 450 - 550 nm. The calculated spectra of compound **1** had a significant absorbance up to 550 nm (Figure 14a-ii) whereas, for **4** a significant absorbance below 450 nm was observed (Figure 14b-ii). Comparing the predicted spectra of the model compounds with visible spectra of known red complexes, the

predicted spectra display maximum absorbance at shorter wavelengths than those reported in the literature. [38-40] As is consistent with the red color of the Ti-containing crystals, none of the model compounds show absorbance above the red range of 450-550 nm. Several solvent systems (toluene, DMF, pyridine) were explored with little variation noted in the final observed UV-vis spectra for compound **1** or **4**.

The addition of electron-withdrawing or electron-donating group analogs of **4** resulted in notable differences in the UV-Vis spectra. The cyano-substituted **EW** derivative shows absorbance strictly below 450 nm (Figure 14c-ii), whereas the methoxy-substituted **ED** absorbs up to 550 nm (Figure 14d-ii). This demonstrates that the 4-MP substituents can affect the color of the crystal, suggesting ligand-to-metal charge transfer is responsible for the observed color in the Ti complexes.

4. Conclusions

A new family of Group 4 alkoxythiols was successfully synthesized and isolated. These were found to form dinuclear 4MP substituted species that were solvated by the parent alkoxide alcohol $[(HOR)(4MP)_3M(\mu\text{-}4MP)]_2$ (**1**-**3**, **7**-**10**). The use of py as a solvent led to monomeric (**4**- **5**) and dinuclear (**6**) 4MP, py solvated compounds. In some instances, the ability to selectively add 4MP ligands was demonstrated (**9**). For all of the Ti-4MP derivatives, the product was red, which was not observed for any of the Zr or Hf species. Studies with varied thiol locations on the ring (**10** – **12**) did not alter this phenomenon. Based on the simulated and observed UV-vis spectra, it was reasoned that the color was generated due to a

ligand-to-metal charge transfer for Ti that was not available for the larger congeners.

Applications of these precursors to materials systems of interest have been preliminarily investigated. The initial polymers generated with **1** have yielded red colored lenses with yellow ones noted for **2** or **3**. Unfortunately, this manipulation led to a weaker polymeric matrix and alternative precursor types will be necessary. Attempts at using these compounds for core-shell nanoparticles show potential for generating the shell; however, additional work is necessary to optimize the process as a controlled shell did not form.

Supporting information. CCDC 1428635-1428645 contains the supplementary crystallographic data for **1 - 12**. These data can be obtained free of charge via http://www.ccdc.cam.ac.uk/conts/retrieving.html, or from the Cambridge Crystallographic Data Centre, 12 Union Road, Cambridge CB2 1EZ, UK; fax: (+44) 1223-336-033; or e-mail: deposit@ccdc.cam.ac.uk

Acknowledgements. The authors would like to thank Mr. J. M. Sears (Sandia) for technical assistance, the Laboratory Directed Research and Development (LDRD) program at Sandia National Laboratories for support of this program, and the use of the Bruker X-ray diffractometer purchased via the National Science Foundation CRIF:MU award to Prof Kemp of the University of New Mexico (CHE04-43580). Sandia National Laboratories is a multi-program laboratory managed and operated by Sandia Corporation, a wholly owned subsidiary of Lockheed Martin Corporation,

for the U.S. Department of Energy's National Nuclear Security Administration under contract DE-AC04-94AL85000.

References.

[1] C.-H. Lai, M.-Y. Lu, L.-J. Chen, J. Mater. Chem., 22 (2012) 19-30.

[2] D.D. Lekeufack, A. Brioude, A. Mouti, J.G. Alauzu, P. Stadelann, A.W. Coleman, P. Miele, Chem. Commun., 46 (2010) 4544-4546.

[3] Y.A. Ovchenkov, H. Geisler, J.M. Burst, S.N. Thornburg, C.A.J. Ventrice, C. Zhang, J. Redepenning, Y. Losovyj, L. Rosa, P.A. Dowben, B. Doudin, Chem. Phys. Lett., 381 (2003) 7-13.

[4] F. Faccini, H. Fric, U. Schubert, E. Wendel, O. Tsetsgee, K. Muller, H. Bertagnolli, A. Venso, S. Gross, J. Mater. Chem., 17 (2007) 3297-3307.

[5] H.C. Hamaker, Physica, 4 (1937) 1058-1072.

[6] R.G. Chandhuri, S. Paria, Chem. Rev., 112 (2012) 2373-2433.

[7] K.Y. van Berkel, C.J. Hawker, J. Polymer Sci:Part A: Polymer Chem., 48 (2010) 1594-1606.

[8] Conquest Version 1.17, Cambridge Crystallographic Data Centre:support@ccdc.cam.ac.uk or http://www.ccdc.cam.ac.uk [CSD version 5.36 (November 2014)].

[9] T.J. Boyle, T.M. Alam, E.R. Mechenbier, B.L. Scott, J.W. Ziller, Inorg. Chem., 36 (1997) 3293-3300

[10] T.J. Boyle, L.A.M. Ottley, S.M. Hoppe, Inorg. Chem., 49 (2010) 10798-10808.

[11] O.V. Dolomanov, L.J. Bourhis, R.J. Gildea, J.A.K. Howard, H. Puschmann, J. Appl. Cryst., 42 (2009) 339-341.

[12] A.L. Spek, Acta Cryst., D65 (2009) 148-155.

[13] M.J. Frisch, G.W. Trucks, H.B. Schlegel, G.E. Scuseria, M.A. Robb, J.R. Cheeseman, G. Scalmani, V. Barone, B. Mennucci, G.A. Petersson, H. Nakatsuji, M. Caricato, X. Li, H.P. Hratchian, A.F. Izmaylov, J. Bloino, G. Zheng, J.L. Sonnenberg, M. Hada, M. Ehara, K. Toyota, R. Fukuda, J. Hasegawa, M. Ishida, T. Nakajima, Y. Honda, O. Kitao, H. Nakai, T. Vreven, J. Montgomery, J. A., J.E. Peralta, F. Ogliaro, M. Bearpark, J.J. Heyd, E. Brothers, K.N. Kudin, V.N. Sterovarov, R. Kobayashi, J. Normand, K. Raghavachari, A. Rendell, J.C. Burant, S.S. Iyengar, J. Tomasi, M. Cossi, N. Rega, J.M. Millam, M. Klene, J.E. Knox, J.B. Cross, V. Bakken, C. Adamo, J. Jaramillo, R. Gomperts, R.E. Stratmann, O. Yazyev, A.J. Austin, R. Cammi, C. Pomelli, J.W. Ochterski, R.L. Martin, K. Morokuma, V.G. Zakrzewski, G.A. Voth, P. Salvador, J.J. Dannenberg, S. Dapprich, A.D. Daniels, O. Farkas, J.B. Foresman, J.V. Ortiz, J. Cioslowski, D.J. Fox, Gaussian 09, Revision A.02, in, Gaussian, Inc., Wallingford CT, 2009.

[14] C. Adamo, V. Barone, J. Chem. Phys., 110 (1999) 6158-6170.

[15] J.P. Perdew, K. Burke, M. Ernzerhof, Phys. Rev. Lett., 77 (1996) 3865-3868.

[16] J.P. Perdew, K. Burke, M. Ernzerhof, Phys. Rev. Lett., 78 (1997) 1396.

[17] P.J. Hay, W.R. Wadt, J. Chem. Phys., 82 (1985) 270-283.

[18] W.R. Wadt, P.J. Hay, J. Chem. Phys., 82 (1985) 284-298.

[19] P.J. Hay, W.R. Wadt, J. Chem. Phys., 82 (1985) 299-310.

[20] W.J. Hehre, R. Ditchfield, J.A. Pople, J. Chem. Phys., 56 (1972) 2257-2261.

[21] P.C. Hariharan, J.A. Pople, Theor. Chim. Acta, 28 (1973) 213-222.

[22] M.M. Francl, W.J. Pietro, W.J. Hehre, J.S. Binkley, M.S. Gordon, D.J. DeFrees, J.A. Pople, J. Chem. Phys., 77 (1982) 3654-3665.

[23] R. Bauernschmitt, R. Ahlrichs, Chem. Phys. Lett., 256 (1996) 454-464.

[24] R.E. Stratmann, G.E. Scuseria, M.J. Frisch, J. Chem. Phys., 109 (1998) 8218-8224.

[25] F. Furche, R. Ahlrichs, J. Chem. Phys., 117 (2002) 7433-7447.

[26] S.I. Gorelsky, A.B.P. Lever, J. Organomet. Chem., 635 (2001) 187-196.

[27] S.I. Gorelsky, A.B.P. Lever, J. Organomet. Chem., 659 (2002) 202.

[28] S.I. Gorelsky, SWizard program, in, University of Ottawa, Ottawa, Canada, 2013.

[29] A. Antinolo, R. Fernandez-Galan, N. Molina, A. Otero, I. Rivilla, A.M. Rodriguez, Inorgnica Chimica Acta, 363 (2010) 3489-3497.

[30] T.J. Boyle, R.M. Sewell, L.A.M. Ottley, H.D. Pratt, C.J. Quintana, S.D. Bunge, Inorg. Chem., 46 (2007) 1825-1835.

[31] N.F.o. 4MP, http://webbook.nist.gov/cgi/cbook.cgi?ID=C637898&Mask=80.

[32] D.C. Bradley, H. Chudzynska, M.B. Hursthouse, M. Motevalli, R. Wu, Polyhedron, 13 (1994) 1-6.

[33] T.J. Boyle, L.A.M. Steele, P.D. Burton, S.M. Hoppe, C. Lockhart, M.A. Rodriguez, Inorg. Chem., 51 (2012) 12075-12092.

[34] T.J. Boyle, H.D.I. Pratt, L.A.M. Ottley, T.M. Alam, S.K. McIntyre, M.A. Rodriguez, J. Farrell, C.F. Campana, Inorg. Chem., 48 (2009) 9191-9204.

[35] S.D. Bunge, T.J. Boyle, H.D. Pratt, T.M. Alam, M.A. Rodriguez, Inorg. Chem., 43 (2004) 6035-6041

[36] C.A. Zechmann, T.J. Boyle, D.M. Pedrotty, T.M. Alam, D.P. Lang, B.L. Scott, Inorganic Chemistry 40 (2001) 2177-2184

[37] T.J. Boyle, L.A.M. Steele, D.T. Yonemoto, J. Coord. Chem., 65 (2012) 487-505.

[38] T.-H. Tran, T.-D. Nguyen, Colloids and Surfaces B: Biointerfaces, 88 (2011) 1-22.

[39] S. Mishra, S.P. Ahrenkiel, Journal of Nanomaterials, 2012 (2012) 902491-902491-902496.

[40] G. Vasapollo, L. Longo, L. Rescio, L. Ciurlia, J. Supercrit. Fluids, 29 (2004) 87-96.

List of Tables

Table 1. Data Collection parameters for **1** – **14**.

Compound	**1**	**2**	**3**	**4**
chemical formula	$C_{56}H_{50}O_{10}S_8Ti_2$	$C_{56}H_{50}O_{10}S_8Zr_2$	$C_{58}H_{50}Hf_2O_{10}S_8$	$C_{34}H_{26}N_2O_4S_4Ti$
formula weight	1235.24	1321.88	1496.42	702.71
temp (K)	173(2)	173(2)	173(2)	173(2)
space group	monoclinic P $2_1/n$	monoclinic P 2_1	monoclinic P $2_1/n$	triclinic P -1
a (Å)	14.5063(7)	12.608(3)	14.5308(12)	10.0154(2)
b (Å)	11.1206(4)	17.067(3)	11.1754(9)	18.4285(10)
c (Å)	20.6667(8)	15.344(3	21.0017(17)	20.3132(11)
α (deg)				108.778(3)
β (deg)	91.1880(10)	112.458(9)	92.309(5)	102.582(3)
γ (deg)				92.917(3)
V (Å^3)	3331.2(3)	3051.3(11)	3407.6(5)	3434.5(3)
Z	2	2	2	4
D_{calcd}(Mg/m^3)	1.231	1.439	1.458	1.359
μ,(Mo, Kα) (mm^{-1})	0.539	0.668	3.337	0.532
R1[a] (%) (all data) wR2[b] (%) (all data)	5.58 (8.97) 14.99 (16.26)	6.72 (15.34) 14.96 (22.59)	2.43 (2.87) 9.64 (10.34)	6.72 (10.22) 17.82 (21.43)
Compound	**5**	**6**	**7**	**8**
chemical formula	$C_{34}H_{26}N_2O_4S_4Zr$	$C_{58}H_{42}Hf_2N_2O_{10}S_8$	$C_{54}H_{46}O_{10}S_8Ti_2$	$C_{58}H_{54}O_{10}S_8Ti_2$
formula weight	746.03	1540.39	1207.19	1265.30
temp (K)	173(2)	172(2)	173(2)	173(2)
space group	orthorhombic Fdd2	orthorhombic Pbca	orthorhombic Pbca	Triclinic P -1
a (Å)	46.7858(18)	13.75555(5)	13.1851(17)	10.7566(4)
b (Å)	10.5571(4)	19.6072(7)	20.202(3)	12.2982(4)
c (Å)	14.1458(5)	22.0627(9)	22.020(3)	16.1793(6)
α (deg)				107.048(2)
β (deg)				94.876(2)
γ (deg)				110.902(2)
V (Å^3)	6986.9(5)	5950.5(4)	5865.4(13)	3180.9(2)
Z	8	4	4	1
D_{calcd}(Mg/m^3)	1.418	1.719	1.367	1.125
μ,(Mo, Kα) (mm^{-1})	0.592	3.826	0.610	0.482
R1[a] (%) (all data) wR2[b] (%) (all data)	2.90 (3.54) 8.75 (11.19)	2.82 (4.90) 11.31 (15.99)	7.86(18.64) 17.79(24.46)	8.86(10.81) 26.74(27.84)
Compound	**9**	**10**	**11[c]**	**12**
chemical formula	$C_{54}H_{82}O_{10}S_4Ti_2$	$C_{44}H_{60}O_8S_4Ti_2$	$C_{58}H_{54}O_{10}S_8Ti_2$	$C_{110}H_{106}O_{10}S_{16}Zr_4$
formula weight	1115.24	940.96	1281.26	2465.78
temp (K)	172(2)	173(2)	173(2)	173(2)
space group	monoclinic P $2_1/n$	monoclinic P $2_1/c$	triclinic P -1	triclinic P -1
a (Å)	14.8955(6)	9.8477(7)	10.1635(4)	11.8834(5)
b (Å)	11.0245(4)	23.1028(18)	12.3891(5)	12.107(5)

c (Å)	19.5572(7)	10.9413(8)	14.3098(6)	22.1423(9)
α (deg)			103.900(3)	102.739(2)
β (deg)	97.925(2)	105.907(5)	108.348(3)	101.976(2)
γ (deg)			104.545(3)	90.535(2)
V (Å^3)	3180.9(2)	2393.9(3)	1552.2(2)	3034.7(2)
Z	2	2	1	1
D_{calcd}(Mg/m^3)	1.164	1.305	----	1.349
μ,(Mo, Kα) (mm^{-1})	0.430	0.556	----	0.661
R1[a] (%) (all data) wR2[b] (%) (all data)	9.01 (16.26) 22.67 (26.08)	7.19 (14.00) 17.09 (22.81)	---- ----	6.96 (14.18) 16.50 (20.89)

[a]$R1 = \Sigma \; | |F_o|-|F_c| | / \Sigma |F_o| \times 100$.

[b]$wR2 = [\Sigma \; w (F_o^2-F_c^2)^2 / \Sigma (w |F_o|^2)^2]^{1/2} \times 100$.

[c]The final structure suffered from ligand disorder and only unit cell information is presented

Table 2. Average bond distances (Å) and angles (deg) for **1**– **10** and **12**. Note: For **11**, disorder in the final model lead to unreliable metrical data, so was not included.

Cmpd	M-(MP)	M-(μ-MP)	M-solv
1	1.83	2.06	2.16
2	1.98	2.19	2.31
3	1.96	2.17	2.26
4	1.87	----	2.28
5	1.98	----	2.39
6	1.95	2.15	2.38
7	1.83	2.05	2.16
8	1.83	2.07	2.19
9	1.91	2.07	2.21
10	1.89	2.06	----
12	1.97	2.19	2.26
Cmpd	**MP-M-MP** (trans) and (cis)	**(μ-MP)-M-(μ-MP)**	**MP-M-solv (trans)**
1	164.0 and 98.5	71.5	163.4
2	162.8 and 98.2	69.7	160.6
3	164.3 and 95.5	71.1	160.0
4	161.5 and 96.0	---	174.0
5	164.7 and 97.3	---	169.2
6	160.5 and 97.3	70.5	178.2
7	163.4 and 97.7	71.7	164.9
8	162.8 and 95.5	72.1	164.0
9	------- and 85.2	71.3	162.8
10	------- and 86.8	73.7	----
12	164.8 and 96.2	70.5	161.1

---- not present in the compound

List of Figures

Figure 1. Structure plot of **1**. Thermal ellipsoids are drawn at 30 % level. Hydrogen atoms have been removed for clarity.

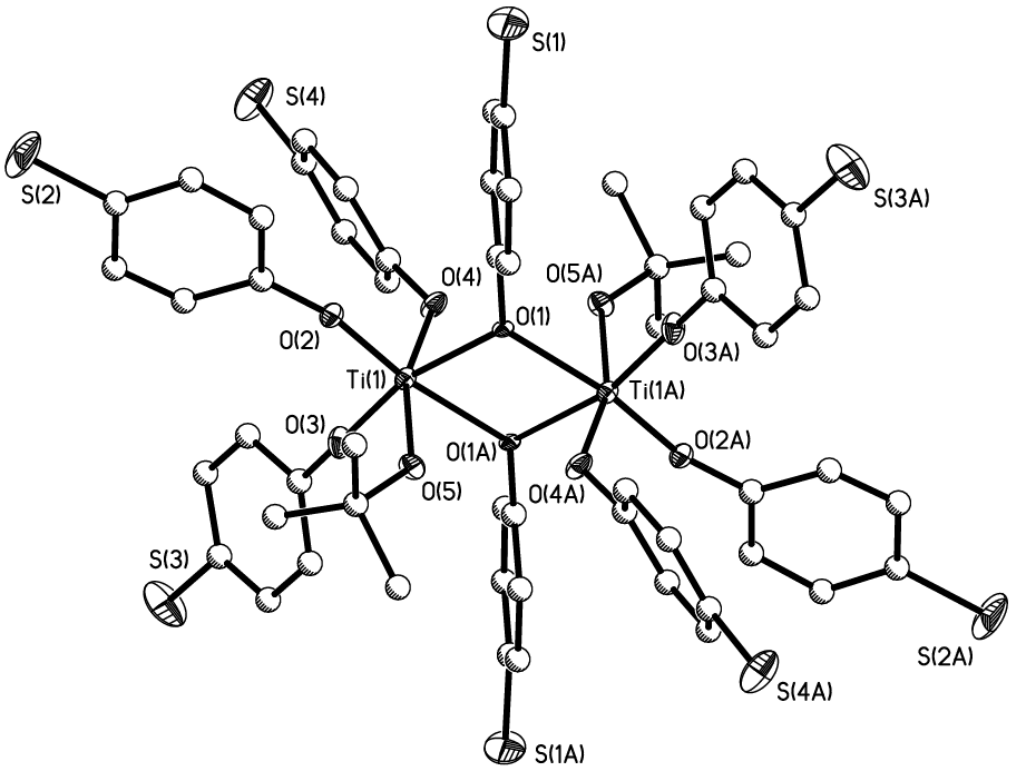

Figure 2. Structure plot of **2**. Thermal ellipsoids are drawn at 30 % level. Hydrogen atoms have been removed for clarity.

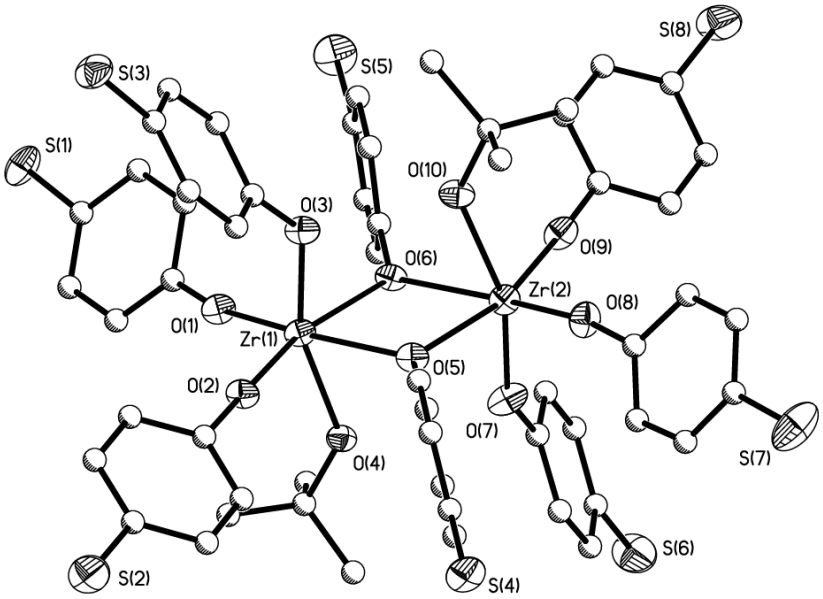

Figure 3. Structure plot of **3**. Thermal ellipsoids are drawn at 30 % level. Hydrogen atoms have been removed for clarity.

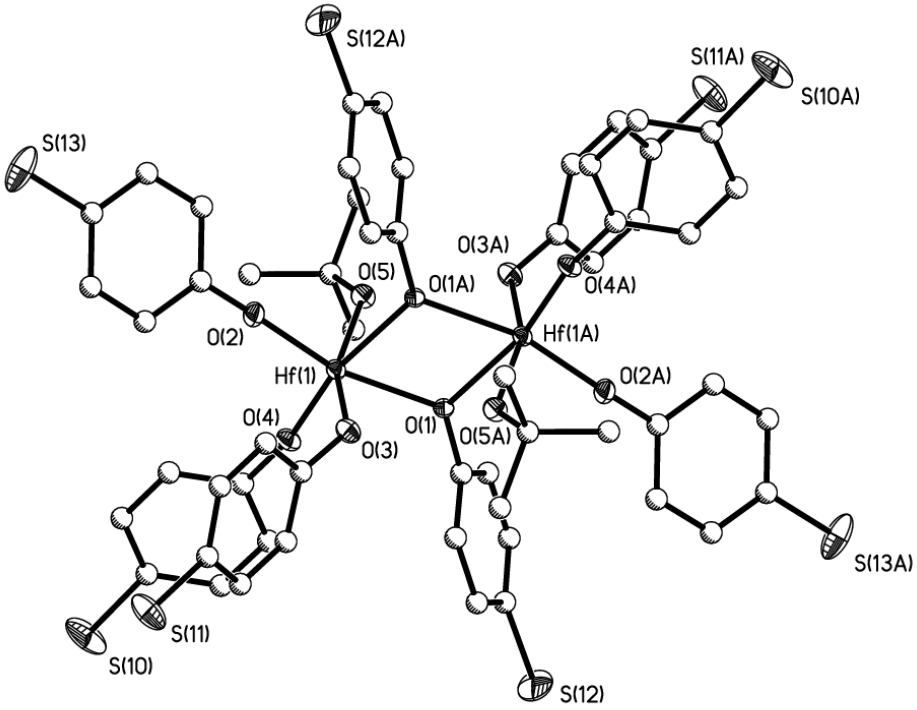

Figure 4. Structure plot of **4**. Thermal ellipsoids are drawn at 30 % level. Hydrogen atoms have been removed for clarity.

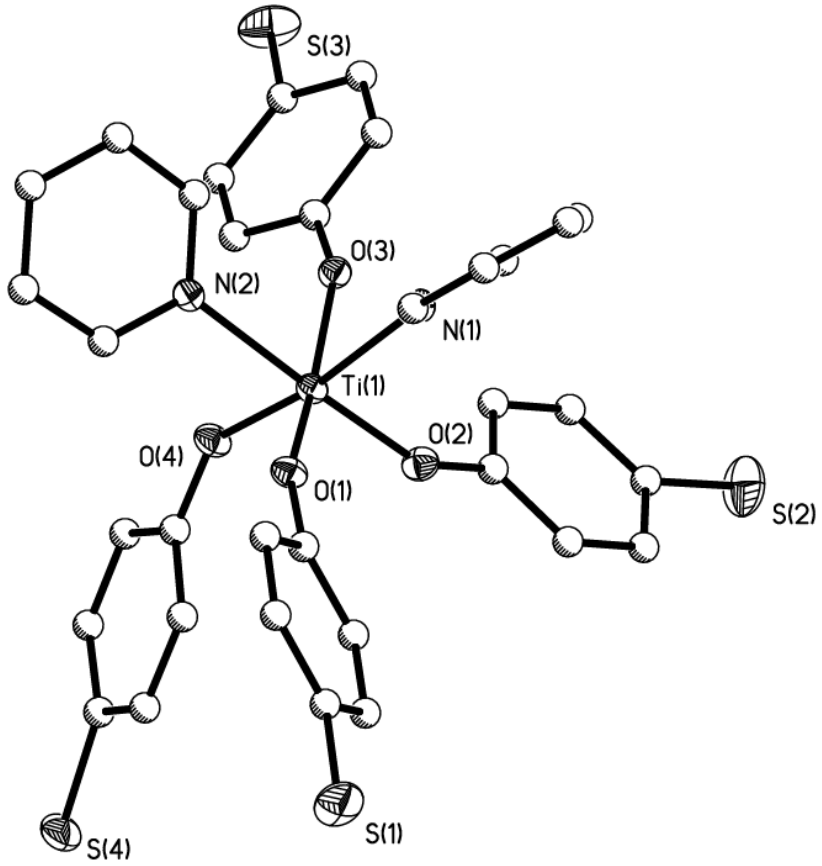

Figure 5. Structure plot of **5**. Thermal ellipsoids are drawn at 30 % level. Hydrogen atoms have been removed for clarity.

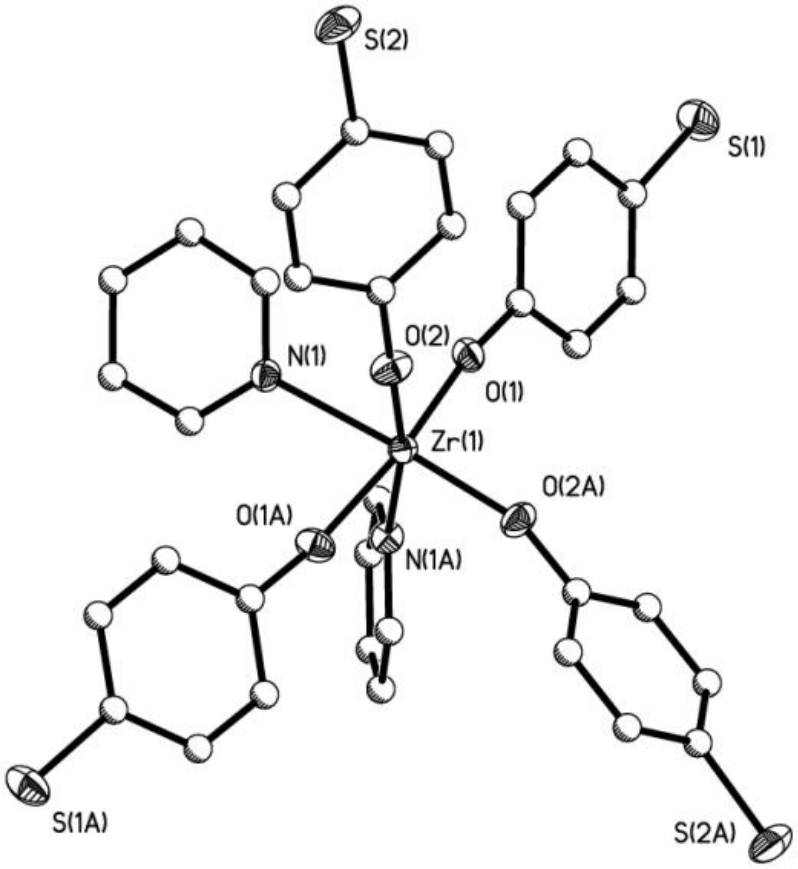

Figure 6. Structure plot of **6**. Thermal ellipsoids are drawn at 30 % level. Hydrogen atoms have been removed for clarity.

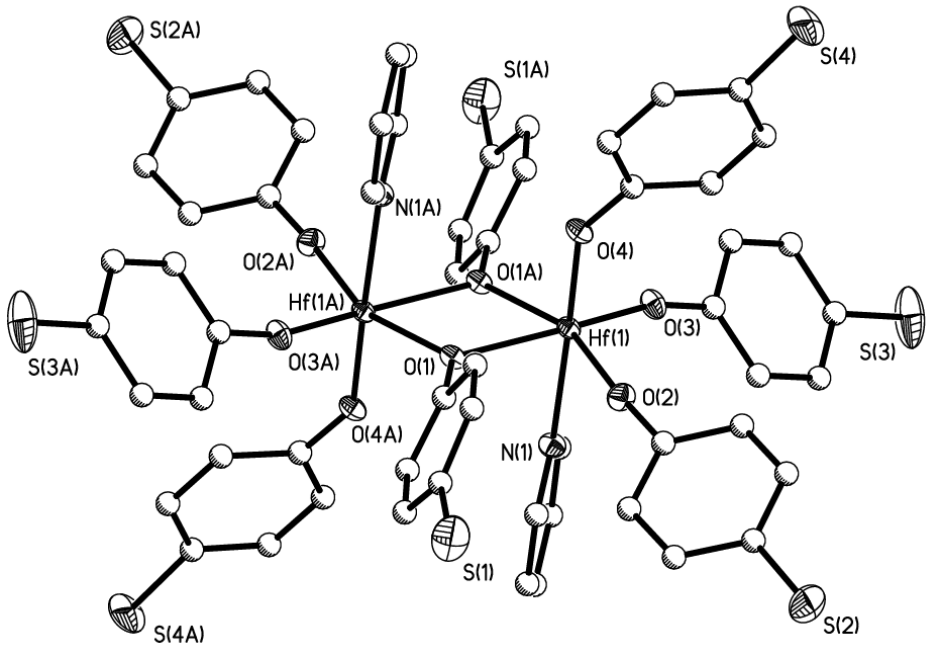

Figure 7. Structure plot of **7**. Thermal ellipsoids are drawn at 30 % level. Hydrogen atoms have been removed for clarity.

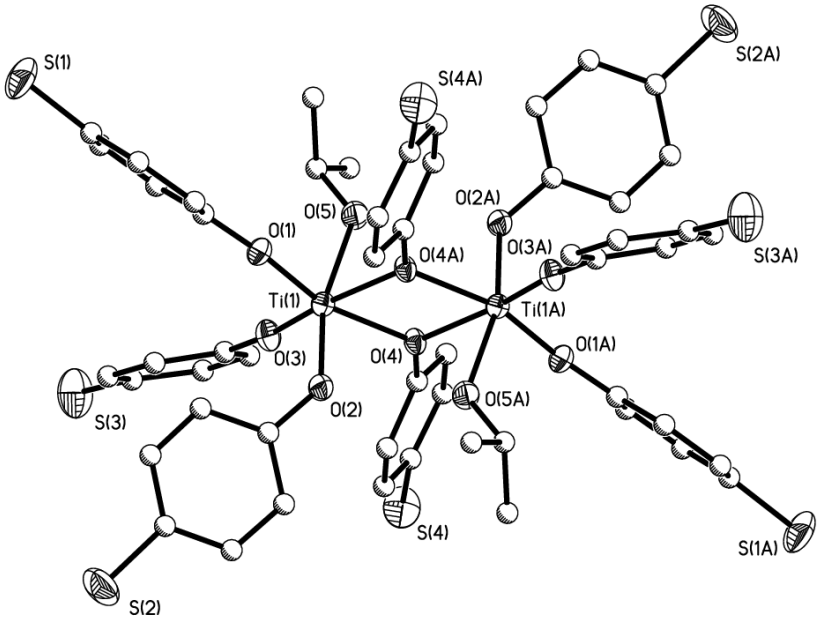

Figure 8. Structure plot of **8**. Thermal ellipsoids are drawn at 30 % level. Hydrogen atoms have been removed for clarity.

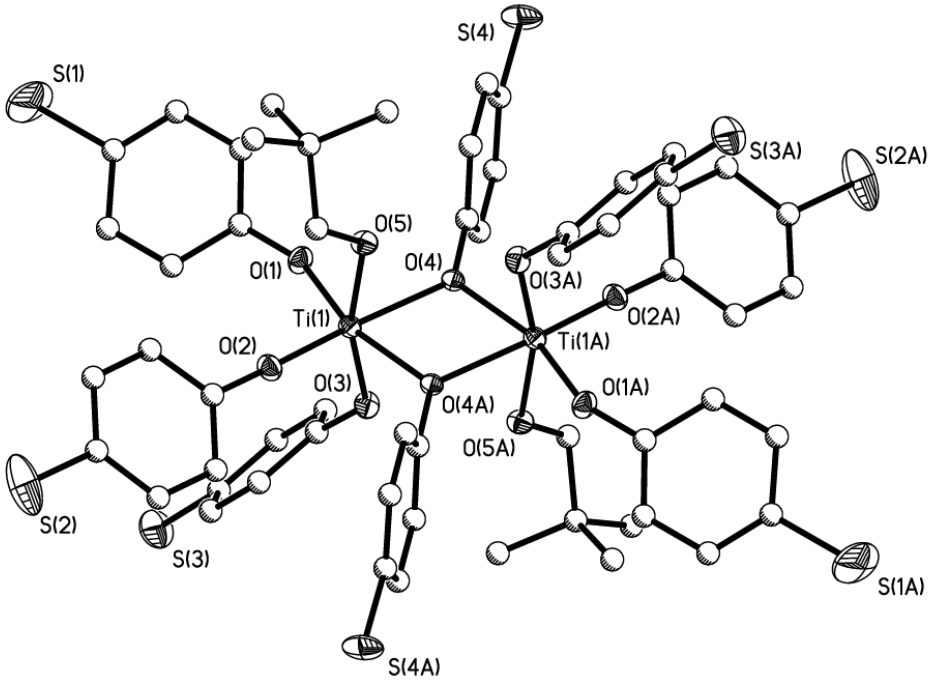

Figure 9. Structure plot of **9**. Thermal ellipsoids are drawn at 30 % level. Hydrogen atoms have been removed for clarity.

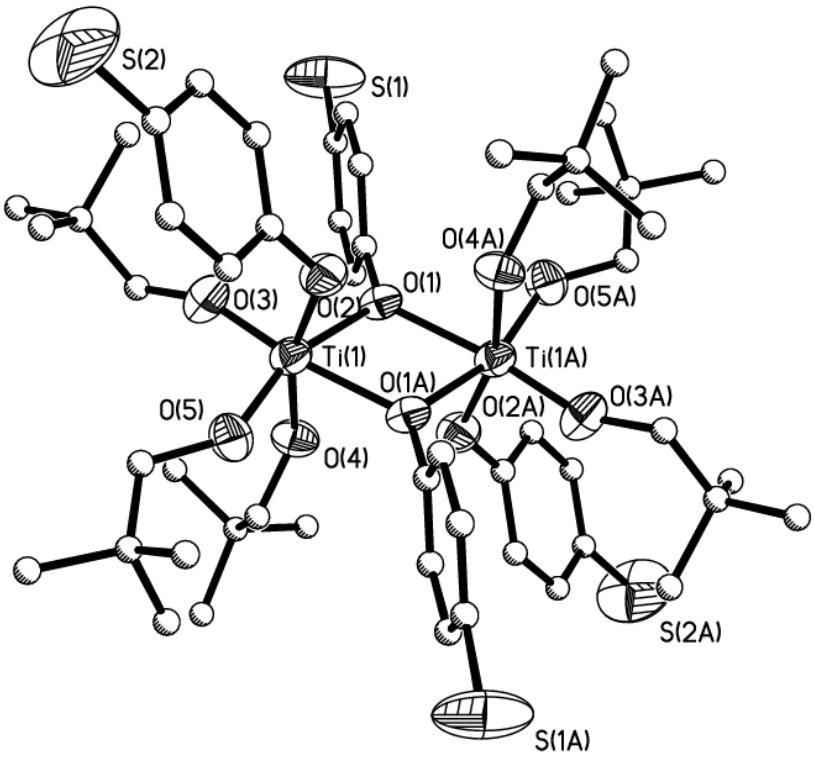

Figure 10. Structure plot of **10**. Thermal ellipsoids are drawn at 30 % level. Hydrogen atoms have been removed for clarity.

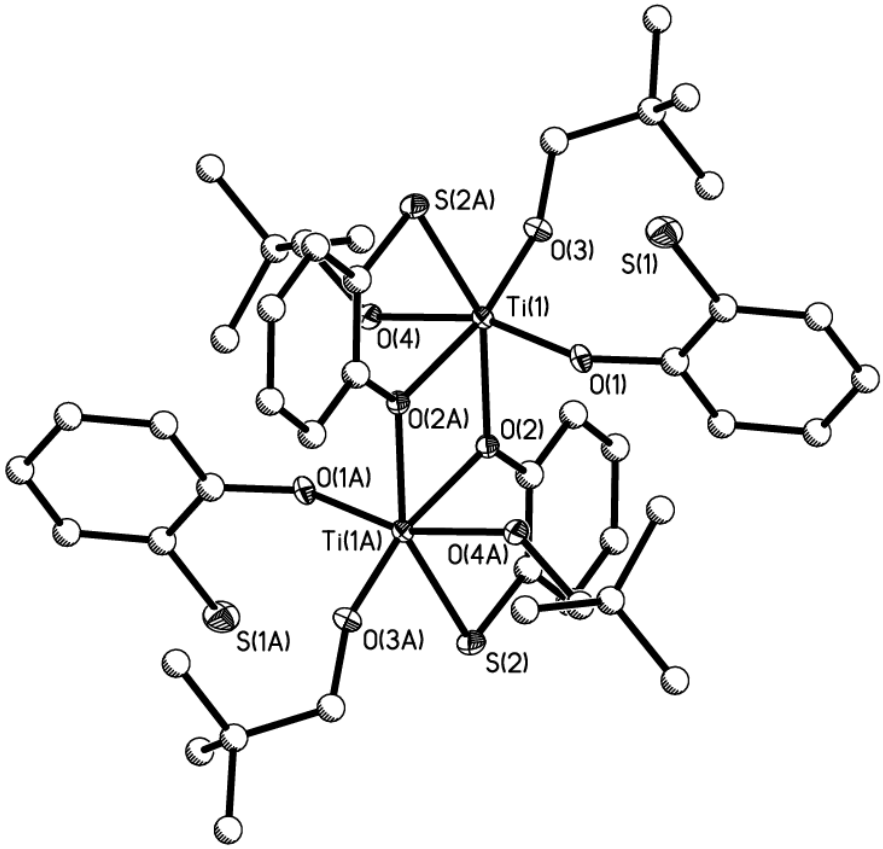

Figure 11. Structure plot of **11**. Thermal ellipsoids are drawn at 30 % level. Hydrogen atoms have been removed for clarity.

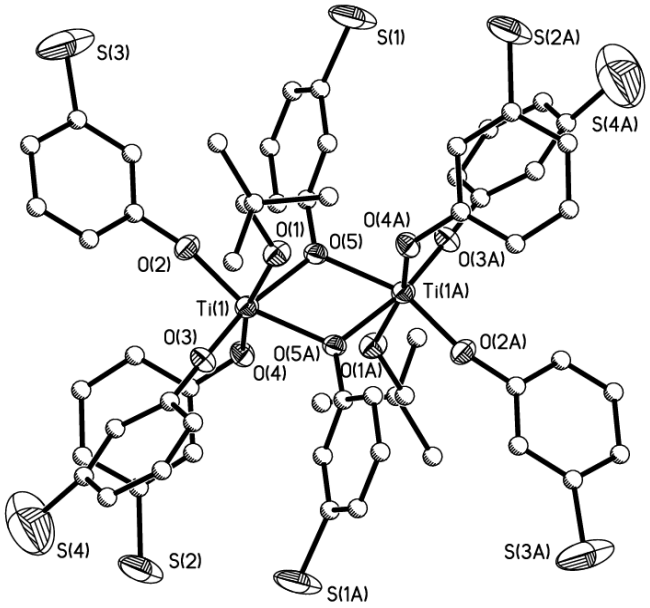

Figure 12. Structure plot of **12**. Thermal ellipsoids are drawn at 30 % level. Hydrogen atoms have been removed for clarity. Two molecules solved per unit cell.

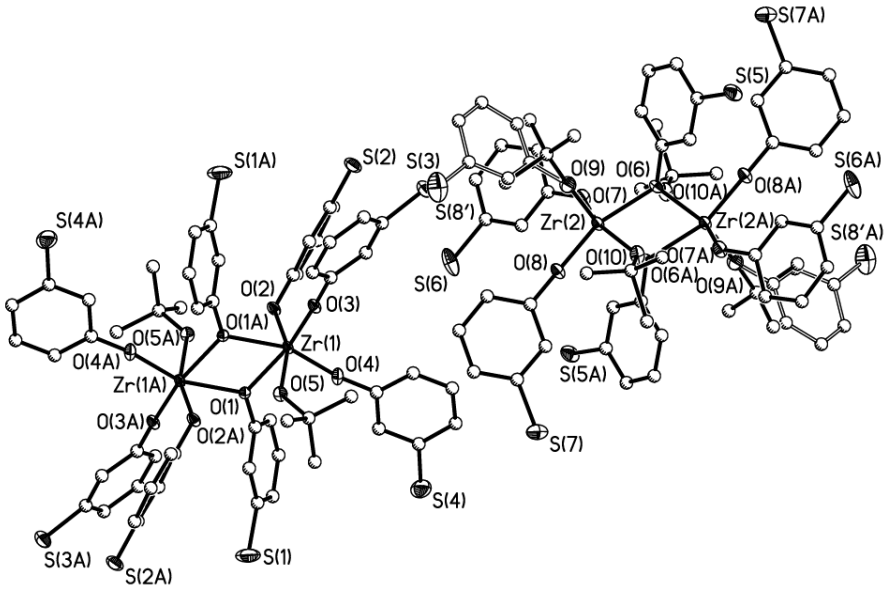

Figure 13. UV-vis spectrum for (a) **1** and (**4**).

(a)

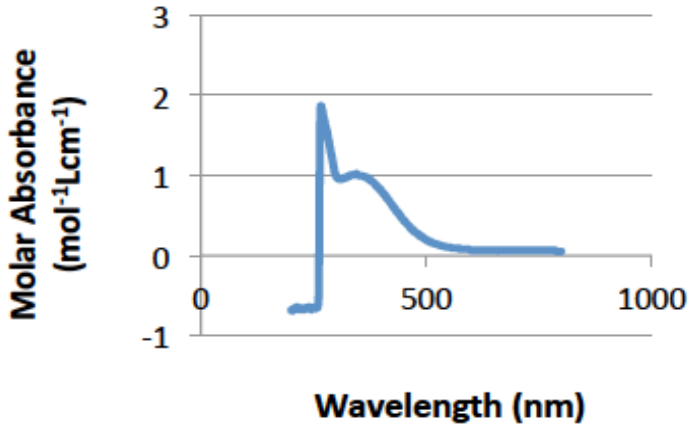

(b)

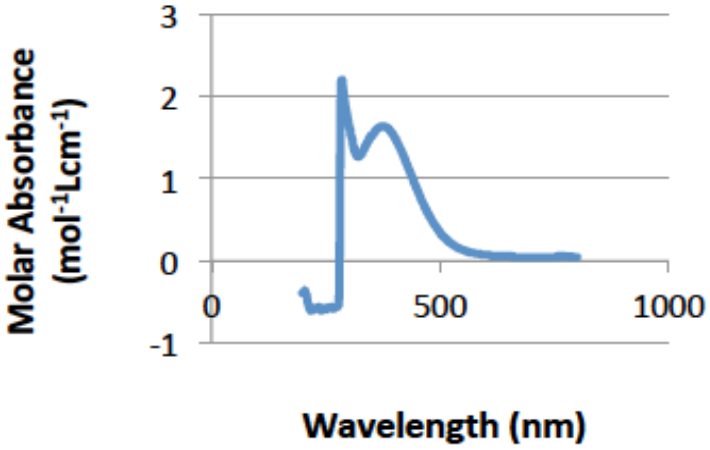

Figure 14. UV-vis spectra analysis: row (a) **1**, (b) **4**, (c) **EW**, and (d) **ED**; Column (i) structure of model compounds and (ii) calculated UV-vis spectrum. Color code: Ti (green), O (red), S (yellow), N (blue), C (black), and H (white)